



Towards a microMRI atlas of mouse development

R.E. Jacobs*, E.T. Ahrens, M.E. Dickinson, D. Laidlaw

Beckman Institute and Division of Biology, California Institute of Technology, Pasadena, CA 91125, USA

Received 3 September 1998; accepted 3 September 1998

Abstract

This study investigates the potential of microscopic Magnetic Resonance Imaging to obtain information for 3D digital atlases of mouse development using fixed samples. Fixed samples allow direct comparison with already published atlases and provide a testing ground for future in vivo efforts. 3D MR images of mouse embryos (dpc 6.5–16) illustrate that the necessary contrast and level of detail is available with this technique. Diffusion weighted imaging, diffusion tensor imaging, and multi-valued data sets are presented as examples of uniquely MR methods of obtaining anatomical information. MRI is performed non-invasively on the intact sample, leaving open the possibility of other manipulations (e.g. classical histology, immunohistochemistry, in situ hybridization, and in vitro growth for unfixed samples) after conducting the MRI experiment © 1999 Elsevier Science Ltd. All rights reserved.

Keywords: MRI; Atlas; Mouse embryo; Morphogenesis; Multi-valued imaging; Development; Diffusion

1. Introduction

Atlases of normal mouse development have immense pedagogical value and provide researchers studying normal, mutant, and transgenic mice a standard against which specific examples may be compared and contrasted. Microscopic Magnetic Resonance Imaging (μ MRI) provides a means of digitally recording anatomical information in three dimensions from intact specimens at reasonable temporal and spatial resolution. This method can be used to image both fixed and live specimens. Moreover, unique contrast mechanisms can be exploited to highlight different features of the specimens. Standard methods of atlas construction typically involve sacrificing, fixing, sectioning, staining, then recording photomicrographs of individual sections. Photographic plates are the raw material of most atlases and atlases contain two additional critical elements: (1) annotation in the form of graphical reconstructions highlighting important detail; and (2) nomenclature in the form of descriptions and names of discrete structures. Atlases of this type for the mouse have been presented by Rugh [1], Theiler [2], and Kaufman [3]. The advent of powerful inexpensive computers coupled with the ability to conveniently transport large amounts of data (via CD-ROM or over the Internet) are bringing about changes in the way atlases are constructed and in the ways they can be

used. When in book form, the intrinsically three dimensional animal must be viewed as a series of two dimensional sections. Moreover, the orientations available to the viewer are limited to samples of standard planes of section (e.g. sagittal, coronal, axial). These restrictions make it difficult to follow complex three dimensional structures and hinder comparison of one's own 'oblique' sections with the 'perpendicular' sections found in the atlases. Digital atlases have the potential to obviate both of these vexing problems [4–7]. With the section data reconstructed into three dimensions, highlighting complex structures and computationally sectioning at arbitrary angles becomes possible. Quantitative morphological measurements (volumes, distances, angles) can be accomplished and maps can be generated that amalgamate data from various experimental techniques. Temporal and spatial gene and protein expression patterns, axonal trajectories, patterns of vasculature, and specific neuronal responses to stimuli can all be combined to obtain a *canonical* organism or system. Such a data set could potentially embody all quantitative information known about the animal in a concise framework. Motivated by such benefits, several efforts are underway to generate digital atlases. There is at least one commercially available CD-ROM rat atlas [8] and other less ambitious CD-ROM undertakings [9,10]. A number of World Wide Web sites present a variety of two dimensional data [11] and some aim towards being three dimensional atlases [12].

The major drawback to classical methods of generating three dimensional digital atlases is that the specimen must

* Corresponding author. Tel.: + 1-626-395-2849; Fax: + 1-626-449-5163; e-mail: rjacobs@caltech.edu

be physically deconstructed from its native three dimensions into a series of two dimensional sets of data, and then digitally reconstructed back into three dimensions. The reconstruction back into three dimensions is a non-trivial effort because of artifacts generated during histological processing and the computational expense of aligning a host of individual sections [13–15]. μ MRI is a qualitatively different imaging method that offers a convenient means around these difficulties. In the MRI experiment the signal is digitized essentially as it is being originally observed. μ MR images are conveniently collected in three dimensions from intact samples with sufficient contrast and spatial resolution to identify many anatomical features. For future work, we note that μ MRI is a non-invasive *in vivo* imaging methodology making it possible to repeatedly image the same specimen over time [15–17]. Thus, one has the potential to image an embryo *in vivo*, then analyze it *in vivo* or as a fixed specimen, and then directly compare these data sets.

This study outlines some examples that point out the advantages and disadvantages of using μ MRI to obtain data for three dimensional atlases of mouse development using fixed samples. The use of fixed samples will allow direct comparison with already published atlases and provide a testing ground for future *in vivo* efforts. First we briefly discuss μ MRI methodology with emphasis on how contrast arises in the MR image and may be manipulated by the experimental protocol. Secondly, we present renderings of 3D MR images of mouse embryos (day post coitum 6.5–16) illustrating the contrast and level of detail available with this technique. In this context we discuss MR diffusion weighted imaging, diffusion tensor imaging, and multi-valued data sets as examples of uniquely MR methods of obtaining anatomical information [18,19]. Thirdly, we outline specific shortcomings of μ MRI and possible extensions.

2. Methods

2.1. MR Microscopy

One of the principal advantages of MR imaging is its ability to perform three dimensional non-invasive imaging of optically opaque specimens. One of its principal disadvantages is the intrinsically poor signal to noise ratio (SNR) of the recorded signals. This limits the spatial and temporal resolution of the MR image. Physical limits to the spatial resolution obtainable with MRI have been discussed in detail by a number of workers [20–24]. Estimates of the theoretical limits of resolution in the MR image range from 2 to 0.5 μ m [25,26]. The practical spatial resolution is currently determined by SNR which is often limited by the amount of time available to acquire the image (i.e. the temporal resolution). The challenge in MRI microscopy is to optimize the experimental setup (hardware and software) to overcome the poor intrinsic SNR in order to obtain a

respectable image in a reasonable amount of time. There are a number of ways of recovering this signal loss, including working at high magnetic fields and customizing hardware and software to the samples of interest [15,22]. The success of these methods is substantiated by MR imaging experiments with spatial resolutions of 10 μ m or less that have been achieved by several groups working at field strengths ranging from 4.7 to 14 T [16,25,27].

2.2. Diffusion MRI

Typically, contrast in the proton MR image arises from regional differences in T_1 , T_2 , magnetic susceptibility, and/or proton concentration that in turn arise from regional differences in physical, chemical, and structural properties of the sample. This is used to great advantage clinically because it offers means of differentiating tissue types. In addition, using a voxel-wise measurement of water diffusion rates, MR imaging can be used to gain information about tissue geometry: whether it is isotropic or anisotropic. In white matter of the central nervous system water diffusion is anisotropic; faster along fibers than perpendicular to them. Whereas, in gray matter it is essentially isotropic [19]. Anisotropy in the context of diffusion MRI means that each image voxel containing white matter has a unique set of values for the diffusion rate of water along each spatial direction. Mathematically, diffusion is described by D , a symmetric 3×3 tensor with six independent values corresponding to diagonal and off-diagonal elements or directions. Diffusion anisotropy can be defined as the ratio of the diffusion rates parallel and perpendicular to the fiber orientation. In white matter tracts, the value can reach 2 to 3; whereas, in isotropic gray matter it is roughly unity [19, 28–30].

2.3. MRI Experiment

Proton MR imaging was performed at 11.7 T using a vertical bore (89 mm) Bruker AMX500 micro-imaging system (Bruker Instruments Inc., Billerica, MA). This system utilizes home-built RF probes and a low-noise preamplifier. An Acustar shielded gradient set (Bruker Instruments Inc., Fremont, CA) provides gradient strengths up to 290 G/cm. Images were recorded at 4°C. Three dimensional multi-spin echo imaging protocols [22] were utilized with one to six echoes being accumulated per excitation. Recycle (TR) and echo (TE) times are noted in figures, but typically TR = 800 ms and TE = 10 ms to 200 ms. Data matrices were typically $256 \times 128 \times 128$ points yielding isotropic volume elements (voxels) of size 15–60 μ m depending on the chosen field of view.

Diffusion weighted and diffusion tensor images were obtained as described by Ahrens et al. [35]. Diffusion weighted images (DWIs) were acquired using a multi-slice pulsed gradient spin echo imaging protocol [31,32] with $\delta = 2$ ms and $\Delta = 7.4$ ms, where δ and Δ are the width and separation of the diffusion gradient pulses. For

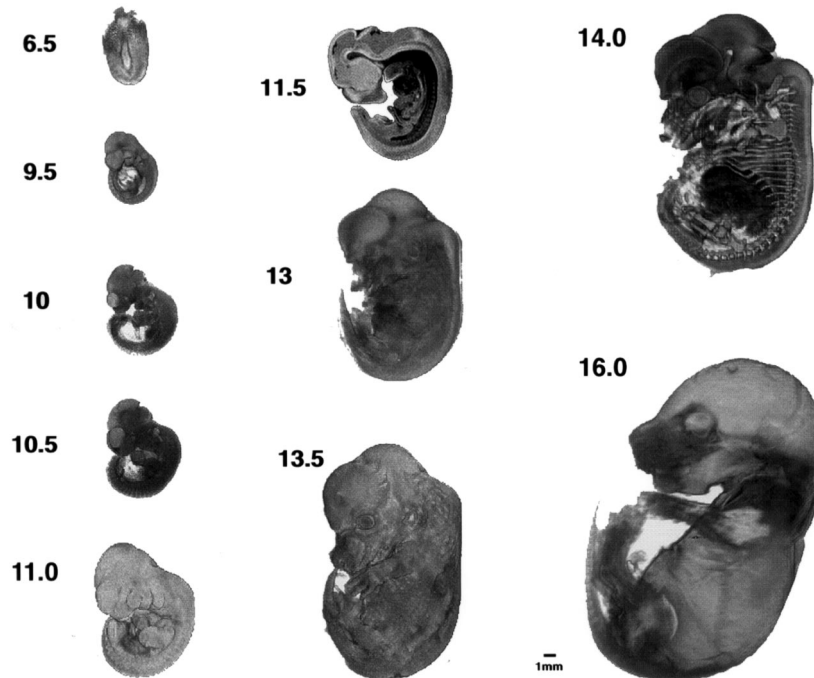


Fig. 1. Volume renderings of 3 dimensional MR images of fixed mouse embryos. Embryo age days post coitum are noted. All data were acquired using a 3DFT spin-echo imaging sequence with TR/TE of 800/10 ms for 6.5 dpc, 900/32 ms for 9.5 dpc, 900/32 ms for 10.0 dpc, 900/32 ms for 10.5 dpc, 500/40 ms for 11.0 dpc, 500/30 ms for 11.5 dpc, 700/32 ms for 13.0 dpc, 800/30 ms for 13.5 dpc and 500/30 ms for 16.0 dpc sample. Only half the volume data is shown for the 6.5 dpc and 11.5 dpc; beginning at the central slice so that internal anatomy is evident. Voxels in the 14.0 dpc image are rendered semi-transparent to show internal anatomy. Orthogonal slice data can be found at <http://muggy.gg.caltech.edu/hbp/atlas/mouse/MouseAtlas.html>.

the diffusion tensor determination a total of 29 DWIs were measured with the same pulse sequence, δ , Δ , but with gradient pulse strengths that varied from 0 to 50 G/cm. The effective diffusion tensor, D , for each voxel was determined using this series of DWIs. The diffusion tensor associated with each image voxel of a DWI satisfies the equation:

$$I = I_0 e^{-bD} \quad (1)$$

where I represents voxel intensity, b represents the diffusion weighting; while I_0 and the diffusion tensor, D , are unknown fit parameters. The diffusion weighting, b , accounts for both the diffusion and imaging gradients and was determined by numerical calculation [32–35]. Bayesian probabilistic fitting techniques were used to solve for I_0 and D in a system of these equations, one for each DWI.

2.4. Animals

Timed pregnancies between C57BL/6J females and DBA/2J males were used to generate embryos at various stages. Noon on the day of the vaginal plug is regarded as 0.5 days post coitum (dpc). Pregnant females were euthanized with CO₂, the embryos were excised and fixed by immersion in 4% paraformaldehyde for 48 hours at 4°C, then washed several times in Phosphate Buffered Saline (PBS) (Sigma). For imaging, the fixed specimen was immersed in PBS or magnetite doped agarose (1% agarose in

PBS, 0.26 mg Fe/ml). The agarose served to maintain the smaller specimens in the center of the RF coil and the magnetite lowered the MR signal intensity of the agarose.

2.5. Visualization

Image visualization was performed on HP9000/755 workstations (Hewlett Packard Inc., Palo Alto, CA) using in-house volume rendering software and SGI workstations (Silicon Graphics Inc., Mountain View, CA) using Voxel-View (Vital Images Inc., Fairfield, IA). Diffusion tensor results were computed using the HP workstations and in-house software.

3. Results

Semi-transparent volume renderings of three dimensional MRI data sets from intact specimens at ten time points are shown in Fig. 1. For the 6.5 and 11.5 day post coitum (dpc) data, rendering begins at a mid-sagittal plane and proceeds backwards into the page, thus only half the information is displayed. For rendering the 14.5 dpc data each voxel was set to be relatively transparent. Both these manipulations serve to reveal internal structure in volume images. For example, the heart, somites, branchial arches, forming limbs, and digits are all apparent in the images. In the other renderings all the data is shown, but each voxel is set to be relatively opaque. The information evident in

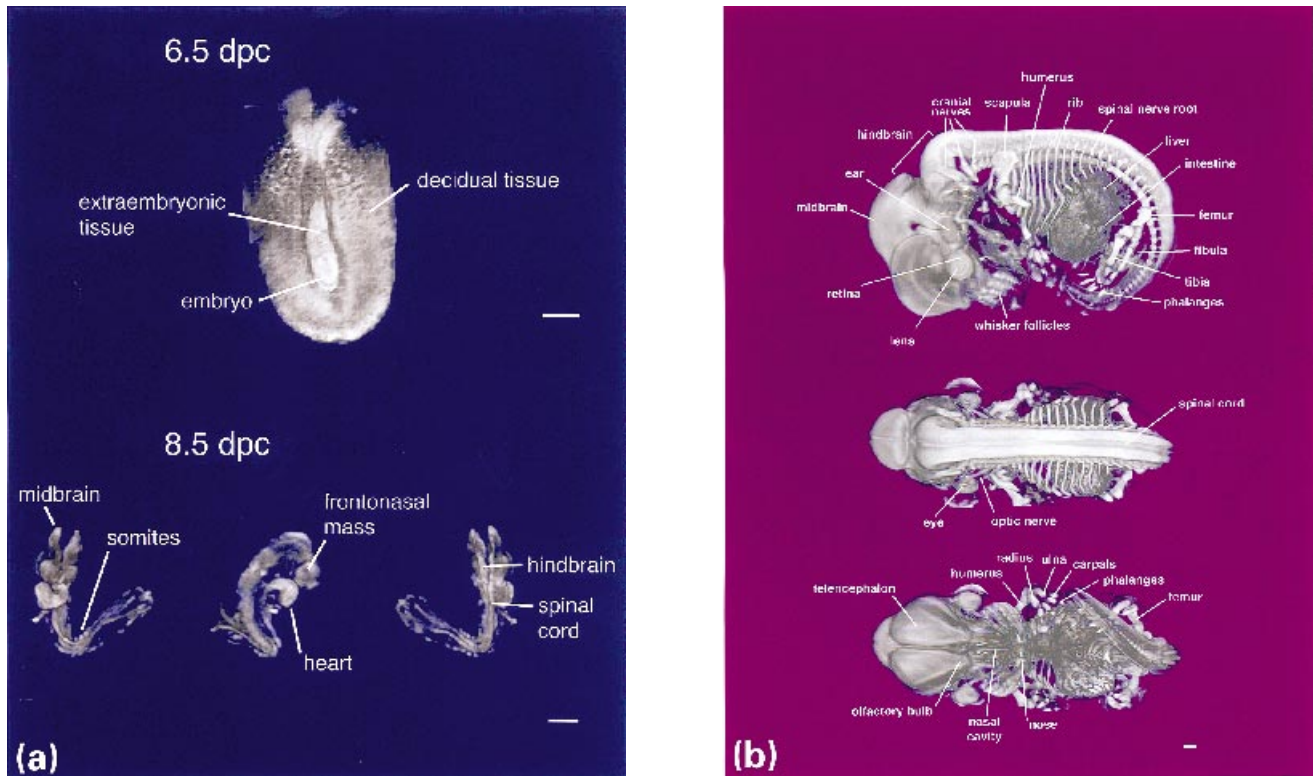


Fig. 2. a. Minimally annotated semi-transparent volume renderings of fixed mouse embryos at 6.5 dpc and 8.5 dpc. Three views of the 8.5 dpc data are shown: left, ventral; middle, side; and right, dorsal. Isotropic voxel resolution is $20\ \mu\text{m}$ in both image, acquired with 3DFT spin echo sequence, $\text{TR}/\text{TE} = 800/10\ \text{ms}$. b. Three annotated semi-transparent views of a 14.0 dpc fixed mouse embryo. Note the similar intensities of large nerves (e.g. cranial nerves) and the not yet ossified skeletal system (e.g. scapula). Non isotropic voxel size of $27 \times 46 \times 46\ \mu\text{m}$, image acquired with 3DFT spin echo sequence, $\text{TR}/\text{TE} = 800/20\ \text{ms}$. Scale bars represents $500\ \mu\text{m}$ in all three cases.

these images is mainly about the surface features of the specimens. Each of the images in Fig. 1 represents one data set from each MR imaging experiment. Not shown are 4 to 6 other coincident MRI data sets for each sample that were recorded with different values of the experimental parameter T_E and offer different contrast.

Fig. 2 shows enlarged and annotated views of 6.5, 8.5 and 14.5 dpc specimens. In the 6.5 dpc sample, the decidua was left intact to investigate the level of contrast between embryonic and extra-embryonic tissue at early stages. Three views of the 8.5 dpc sample are shown in which extra-embryonic tissue has been removed. This specimen has been captured part way through the turning process that is characteristic for mammalian embryos [36]. This semi-transparent volume rendering clearly reveal structures such as the heart, somites, midbrain, hindbrain, and spinal cord. A large number of features are identifiable in the 14.5 dpc image, not all of which are labeled nor are visible in this rendering. The developing skeletal system is still primarily cartilaginous at this time [5]. Thus, it is not hypointense as is the case in typical MR images of the adult animal skeletal system [37]. In this image the signal intensity from the skeletal system is similar to that arising from the nervous system (e.g. compare cranial and spinal nerves to the adjacent scapula in the upper sagittal view).

Volume renderings and para-sagittal sections from six different, yet spatially coincident, MRI data sets of a 10.5 dpc embryo are shown in Fig. 3. The images were recorded in a single imaging session. The five images with T_E values varying from 10 to 50 ms were recorded during a single multi-echo acquisition protocol and the diffusion weighted image was recorded immediately following it. Taken together these data sets comprise a single multi-valued data set where each voxel has six values associated with it. The $T_E = 10\ \text{ms}$ image is essentially a proton density weighted image where contrast is low due to the relatively uniform water concentration. The longer T_E -valued images show increased intensity differences in different parts of the embryo and a decrease in overall SNR with increasing T_E . The diffusion weighted image was recorded with diffusion gradients in the anterior-posterior direction causing a decrease in signal from water motion in that direction. Thus, contrast originates from qualitatively different mechanisms than that obtained in the T_2 weighted images.

The depiction of multi-valued data in a two or three dimensional format is a formidable problem. There are several techniques for reducing the dimensionality of the problem. One is simply to view the components individually as in Fig. 3. Another is to perform a principal component analysis or eigenimage filtering methods [38] and view the

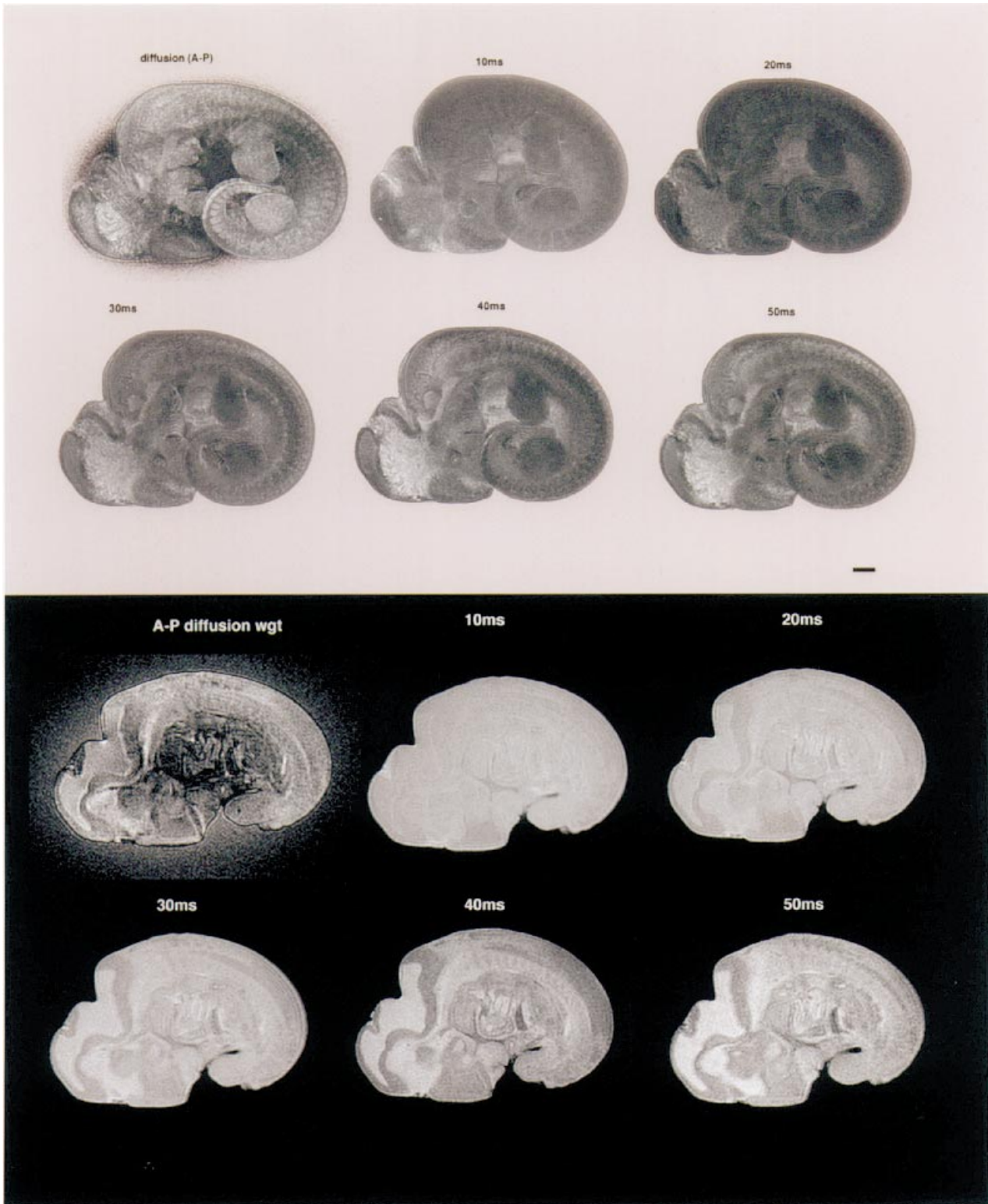


Fig. 3. Fixed mouse embryo 10.5 dpc represented in a multi-valued 3D MRI data set. Top panel show semi-transparent volume renderings, while bottom panel shows para-sagittal slices through the data. Diffusion weighted image in the upper left was acquired with a 2D version of PGSE sequence with $TR/TE = 800/30$ ms, $\delta = 4$ ms and $\Delta = 24$ ms, where δ and Δ are the width and separation of the gradient pulses. Gradient strength was 16 G/cm and direction was along the long axis of the specimen. The remaining 5 images were acquired with a multi-echo SE sequence with the echo times noted of 10 ms through 50 ms. Isotropic voxel resolution is 40 μm for all images. Diffusion weighted image was recorded immediately after the multi-echo experiment with identical magnitude and direction of the position encoding gradients. These six data sets are spatially coincident. Each voxel may be thought of as contain six values.

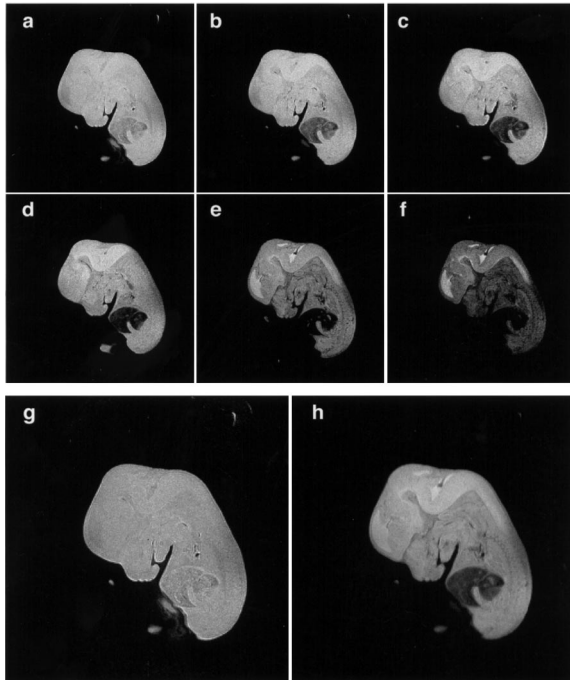


Fig. 4. Slices of six-valued mouse embryo magnetic resonance volume imaging data (a–f). Each image shows one component of the six-valued data. For panels (a–f), TE = 10, 20, 30, 40, 50 and 100 ms, respectively; and TR = 1000 ms for the 3D spin-echo MRI acquisition. (g) and (h) show two different linear combinations of the images in (a–f). The combinations were chosen to satisfy goals that would make them particularly effective for volume-rendering. The first, (g), creates a mask for specimen versus surroundings and the second, (h), contrasts different materials optimally. Both achieve the intensity goals while keeping noise below a specified level.

individual components. A new technique, illustrated in Figs. 4 and 5, shows slice and volume images created as linear combinations of the six spatially coincident volume images based on particular specified goals [39]. The original MR data were acquired as two multi-echo acquisitions, one of

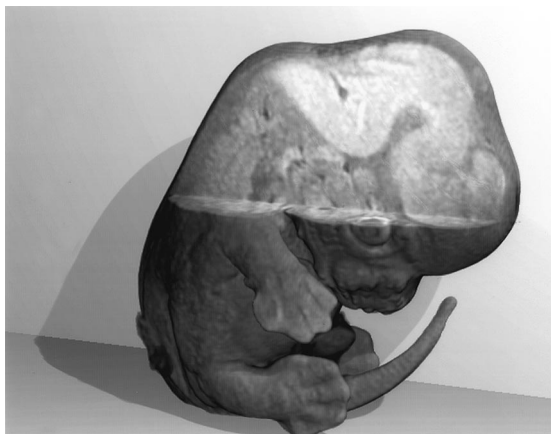


Fig. 5. Volume rendering created from the optimal linear combinations shown in Fig. 4. The surface of the embryo is well-defined by the mask combination and the interior materials well distinguished in the cutaway portion of the image.

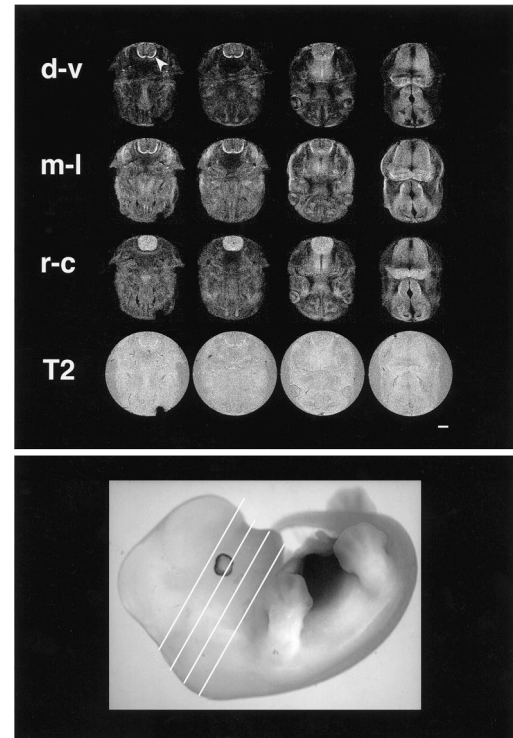


Fig. 6. Multi-slice transverse diffusion weighted images through the brain and spinal cord of the 12.5 dpc mouse embryo whose optical image is shown in the lower panel. Slice locations are noted in the optical image. Each column shows the same slice with the left column being the most posterior slice. Each row shows a different experimental condition: d–v, diffusion weighting in dorsoventral direction; m–l, diffusion weighting in mediolateral direction; r–c, diffusion weighting in rostrocaudal direction; T2, diffusion gradients set to zero. In all DWIs the gradient strength was 32G/cm, $\delta = 2$ ms and $\Delta = 7.4$ ms. In all 16 slices the thickness was 300 μm with in-plane resolution of $20 \times 20 \mu\text{m}$ and TR/TE = 2000/17 ms. Scale bar is 500 μm . The pre-myelinated fiber tracts in the marginal zone (arrowhead) of the spinal cord are hyperintense in the dorsoventral and mediolateral diffusion weighted slices, but not the rostrocaudal diffusion weighted slice.

four echoes ($T_E = 10, 20, 30, 40$ ms), and one of two echoes ($T_E = 50, 100$ ms). Sections through the initial images are shown in Fig. 4(a–f). Weighting factors for each of the six MR data sets were chosen to make a linear combination image that satisfied goals leading to clear, meaningful volume renderings. Two linear combinations were created. The first combination was a “mask” value, used as opacity in the rendering process. To begin, a small set of representative points in the images from five different regions of interest within the embryo were selected. A combination of images was then chosen in which one could utilize the black signal outside the embryo and a constant value inside the embryo. The best images had sufficient signal-to-noise ratio (SNR) between black and the constant value. A second combination was chosen to map different materials to equally spaced intensities with a sufficient contrast-to-noise ratio. Sections through the resulting combination images are shown in Fig. 4(g) and (h) and a volume rendering using the combination images in Fig. 5.

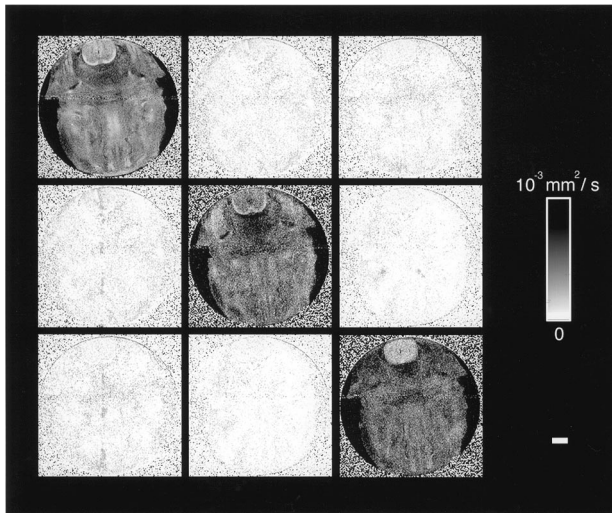


Fig. 7. Diffusion tensor elements (D_{ij}) from the most rostral slice in Fig. 6. The elements were obtained from a non-linear fit of Eq. (1) using a total of 29 diffusion weighted images. Experimental parameters were as for the images in Fig. 4 with a variety of gradient directions and strengths ranging from 0 to 50 G/cm. Scale bar is 500 μm . Diagonal tensor elements reveal the large amount of diffusion anisotropy present in the marginal zone of the spinal cord.

Fig. 6 shows diffusion weighted images of a 12.5 dpc mouse embryo with diffusion weighting in each of three mutually perpendicular directions. The four slices were recorded at the locations shown in the optical image (Fig. 6 lower panel). Each column shows the same slice, where each image in the column is weighted by diffusion gradients applied along the dorsoventral, mediolateral, and rostrocaudal directions. The bottom row shows T_2 and proton density weighted images that were acquired using the same experimental conditions as the diffusion weighted data, except that the diffusion gradients were set to zero. Pre-myelinated fiber tracts in the marginal zone of the spinal cord are clearly visible as hyperintense areas in the dorsoventral and mediolateral diffusion weighted images. With the diffusion gradients applied along the rostrocaudal direction, the entire spinal cord has relatively uniform intensity. To quantify the water diffusive motion in this sample, the entire effective diffusion tensor was measured. The results of this measurement are shown in Fig. 7 for the most posterior slice of Fig. 6. Differing intensities of the diagonal elements in the marginal zone indicate a significant amount of diffusional anisotropy. Using MR to obtain diffusion weighted and diffusion tensor images offers a means to access the characteristics of water diffusion on a voxel by voxel basis. Therefore, we can obtain information about the microstructure of the underlying tissue.

4. Discussion

The goal of the present work is to assess the usefulness of μMRI in constructing digital atlases of mouse development.

Such atlases require three dimensional data recorded at a number of time points during development. The data must have sufficient spatial resolution, SNR, and contrast to enable different tissues and organs to be distinguished. In fixed samples where motion is not a consideration, the attainable spatial resolution is largely determined by the desired SNR in the final image which is determined by the experiment time. Thus, there is a definite trade-off between resolution, SNR, and experiment time. Experiment times of 12–25 hours afford the quite reasonable SNR seen in Figs. 1–7. Spatial resolution in these MR images is somewhat coarser than that employed in the atlases of Theiler [2], and Kaufman [3]; ranging from 15 μm in the younger embryos to 60 μm in the oldest specimens. Nevertheless, many anatomical details are evident at 15 μm resolution in the 8.5 dpc specimen of Fig. 2(a) (e.g. individual somites) and at 30 μm resolution in the 14 dpc image of Fig. 2(b) (e.g. structures in the eye). If it proves necessary, spatial resolution of 15 μm is experimentally attainable for all the sample sizes imaged in this study, but at the expense of longer experiment times and significantly larger data sets.

In a physically sectioned embryo, tissue types are typically distinguished by histological staining methods. In the MR images presented in this work no extrinsic stains have been added to the specimens. Instead, the ‘stains’ reside in the intrinsic physical nature of the tissues that modulate the MR signal. T_2 and diffusion weighting are two ways of ‘developing’ these intrinsic ‘stains’ that accentuate the differences in the properties of the different parts of the sample. The labor required to go from fixed sample to the 3D digital MR image is minimal when compared to the analogous histological process. Furthermore, MR contrast agents offer a potential means to alter the MR image intensity in particular parts of the sample by the addition of exogenous agents [40,41]. MR contrast agents are more obviously analogous to the stains employed in histological labeling as they are exogenous compounds added to the preparation in order to differentiate one part of the specimen from another. Strategies involving such contrast agents are currently being pursued to determine specificity for different regions of the embryo [10,42–44].

In some cases the intensity level of one tissue type in a single image may be quite similar to a distinctly different tissue type (e.g. portions of the skeletal system and nervous system seen in Fig. 2(b)). Although *a priori* knowledge of the expected location and shape of the different tissues may allow their discrimination, different experimental parameters may provide another image in which the tissues of interest have significantly different intensities. Determining the set of experimental parameters that will provide the optimal image is not a trivial matter due to the large number of parameters that effect the image intensity and will depend strongly on the goals of the viewer. This difficulty is compounded by the rapid cell differentiation and morphological changes that take place early in development that can be accompanied by local changes in T_1 , T_2 , D , and water

concentration. Thus, an optimal set of experimental parameters for imaging a 8.5 dpc specimen may be different from the optimal set for imaging a 16.5 dpc specimen. We have adopted the approach of recording multiple spatially coincident data sets, then choosing the most appropriate one and or mathematically combining them to take advantage of all the information contained in the multi-valued data. Fig. 3 shows representations of a multi-valued MRI data set demonstrating that even relatively minor changes in experimental parameters (i.e. T_E variation from 10 to 50 ms) has significant effects on MR image contrast. Moreover, the diffusion weighted images (Fig. 6) provide contrast of a fundamentally different variety: signal is suppressed in regions with the most rapid diffusion along the anterior–posterior direction. Analysis of multi-valued data sets (Figs. 4 and 5) will aid in discrimination of tissues that display similar intensities at a single set of experimental parameters.

In an atlas of development it is essential to include information about the characteristics of structures, tissues, organs, as well as information about their sizes, shapes, and locations. The variety of physical mechanisms that give rise to contrast in the MR image and the versatility of the technique make it possible to access local properties of water that are modulated by the underlying characteristics of the tissues. For example, fiber tracts are strongly anisotropic, having roughly cylindrical symmetry. Water diffusion in this anisotropic environment is also anisotropic: diffusion along the fiber bundle is relatively rapid compared to the rates perpendicular to the bundle direction. In the case of injured or diseased fiber tracts the local environment can become less anisotropic and water diffusion becomes more isotropic [35]. In Fig. 6 diffusion weighted MR imaging is used to delineate the initial phases of the formation of fiber tracts in the marginal zone of the mouse embryo spinal cord. The strongly oriented, but not yet myelinated, tracts in the marginal zone appear bright in DWIs when the diffusion gradients are perpendicular to the tract direction (dorso-ventral and mediolateral). This is because the effective diffusion coefficient perpendicular to the tract direction is significantly smaller than that parallel to the tract direction or that in the surrounding tissue. Thus, signal strength in the marginal zone is less effected by these diffusion sensitizing gradients. The diffusion tensor image confirms that water diffusion in the marginal zone where fibers mostly align along the length of the spinal cord (D_{zz} direction) is significantly more rapid than in either perpendicular direction (D_{xx} and D_{yy} components). Because the images showing diffusional anisotropy are spatially coincident with the anatomical images, this information can be directly overlaid onto a digital atlas.

As pointed out by Kaufman & others [4–6,45–47], two important utilities of a 3D digital atlas are the ability to delineate anatomical domains on a voxel-by-voxel basis (i.e. ‘‘paint in’’ structures) and to overlay information from other sources. Gene expression domains, metabolic

activity, cell lineage, and any other information whose spatial and temporal distribution is known could be incorporated into the anatomical atlas. A digital atlas of the type envisioned here could serve as the repository for a host of different spatial data and allow spatio-temporal correlations among the different classes of information. μ MR imaging offers the opportunity of obtaining 3D anatomical images of the *same* sample that would subsequently be analyzed via standard destructive histological procedures for other information of interest. Transferring this information to the sample’s own anatomy (stored as a three dimensional MRI data set) is much more straightforward than mapping onto some arbitrary individual or average representation of mouse anatomy.

5. Summary

The images presented here and by others [10] demonstrate that the resolution and contrast attainable with μ MR imaging are sufficient to allow identification of many tissues and organs within the developing mouse embryo. The three dimensional digital nature of μ MRI obviates the problems associated with the digitization of tissue sections of a physically sliced sample, correction for distortions, and reconstruction back into three dimensions. This leads to a large savings in time and effort compared to the histological route, which is much more labor intensive. The non-invasive character of MR imaging leaves open the possibility of other manipulations (e.g. classical histology, immunohistochemistry, in situ hybridization, and in vivo growth for unfixed samples) with the same specimen after conducting the MRI experiment. The 3D MR image can serve as a template on which to guide the reconstruction of a specimen serially sectioned after MR imaging. Diffusion weighted and diffusion tensor imaging provide examples of contrast arising in MR images not available in optical imaging. The vast array of contrast mechanisms and MR imaging methods are additional reasons to employ MRI in mouse atlas work. μ MRI is a rapidly-developing approach to problems in developmental biology with many avenues to pursue. Atlases based on this technology, especially when used in conjunction with other types of analysis, should prove indispensable not only to the researcher using μ MRI, but also to the general scientific community.

Acknowledgements

This work was supported by the Beckman Institute at Caltech, by the Human Brain Project with contributions from the National Institute on Drug Abuse, the National Institute of Mental Health, and the National Science Foundation; and the Damon Runyon–Walter Winchell Cancer Foundation (M.E.D.)

References

- [1] Rugh R. The Mouse. Its Reproduction and Development. Minneapolis: Burgess Publishing Co, 1968 reprinted by Oxford University Press (1990).
- [2] Theiler T. The House Mouse: Atlas of Embryonic Development. New York: Springer-Verlag, 1989 178p.
- [3] Kaufman MH. The Atlas of Mouse Development. London: Academic Press, 1992.
- [4] Williams BS, Doyle M. An Internet atlas of mouse development. *Computerized Medical Imaging and Graphics* 1996;20(6):433.
- [5] Kaufman MH, Brune RM, Baldock RA, Bard JBL, Davidson D. Computer-aided 3-D reconstruction of serially sectioned mouse embryos: Its use in integrating anatomical organization. *International Journal of Developmental Biology* 1997;41(2):223.
- [6] Gibaud B, Garlatti S, Barillot C, Aure E. Methodology for the design of digital brain atlases. *Lecture Notes In Artificial Intelligence* 1997;1211:441.
- [7] Toga AW, Santori EM, Hazani R, Ambach K. A 3D digital map of rat-brain. *Brain Research Bulletin* 1995;38(1):77.
- [8] Paxinos G, Watson C. The Rat Brain in Stereotaxic Coordinates. San Diego: Academic Press, 1997 280p.
- [9] Ghosh P, O'Dell M, Narasimhan PT, Fraser SE, Jacobs RE. Mouse Lemur Microscopic MRI Brain Atlas Neuroimage 1994;1(4):345–349 and CD-ROM.
- [10] Smith BR, Linney E, Huff DS, Johnson GA. Magnetic Resonance Microscopy of Embryos. *Computerized Medical Imaging and Graphics* 1996;20(6):483–490.
- [11] <http://www.med.harvard.edu:80/AANLIB/home.html>; <http://bitmed.ucsd.edu/cybermouse.html>; http://www.nlm.nih.gov/research/visible/visible_human.html; <http://mickey.utmem.edu/Atlas/AtlasIntroFramePage.html>; <http://www.ifts-atlas.org/ifts/index.html>].
- [12] <http://genex.hgu.mrc.ac.uk/>; <http://glengoyne.hgu.mrc.ac.uk/>; <http://www.loni.ucla.edu/data/index.html>; <http://embryo.mc.duke.edu/animal/home.html>; <http://www.muritech.com>].
- [13] Toga AW, Ambach KL, Quinn B, Shankar K, Schluender S. Post-mortem Anatomy. In: Toga AW, Mazziotta JC, editors. *Brain Mapping: The Methods*, New York: Academic Press, 1996. pp. 169.
- [14] Toh M Y, Falk R B, Main J S. Interactive brain atlas with the visible human project data: Development methods and techniques. *Radiographics* 1996;16(5):1201.
- [15] Narasimhan RT, Jacobs RE. Neuroanatomical Micromagnetic magnetic Resonance Imaging. In: Toga AW, Mazziotta JC, editors. *Brain Mapping: The Methods*, San Diego: Academic Press, 1996. pp. 147.
- [16] Jacobs R E, Fraser S E. Magnetic Resonance Microscopy of Embryonic Cell Lineages and Movement. *Science* 1994;263:681–684.
- [17] Smith B R, Shattuck MD, Hedlund L W, Johnson GA. Time-course imaging of rat embryos in utero with magnetic resonance microscopy. *Magnetic Resonance In Medicine* 1998;39(4):673.
- [18] Basser PJ, Pierpaoli C. Microstructural and Physiological Features of Tissues Elucidated by Quantitative-Diffusion-Tensor MRI. *J. of Magnetic Resonance Series B* 1996;111:209–219.
- [19] Le Bihan D, editor. *Diffusion and Perfusion Magnetic Resonance Imaging* New York: Raven Press, 1995.
- [20] Blumich B, Kuhn W, editors. *Magnetic Resonance Microscopy* New York: VCH Publishers, 1992 604p.
- [21] House WV. NMR Microscopy. *IEEE Trans. Nucl. Sci.* 1984;NS-31:570–577.
- [22] Callaghan PT. *Principles of Nuclear Magnetic Resonance Microscopy*. New York: Oxford University Press, 1991.
- [23] Cho ZH, Ahn CB, Juh SC, Jo JM, Friedenber RM, Fraser SE, Jacobs R E. Recent progress in nmr microscopy towards cellular imaging. *Phil Trans Roy Soc London A* 1990;333(1632):469.
- [24] Zhou X, Lauterbur PC. NMR Microscopy Using Projection Reconstruction. In: Blumich B, Kuhn W, editors. *Magnetic Resonance Microscopy*, New York: VCH Publishers, 1992. pp. 3.
- [25] Cho ZH, Ahn CB, Juh SC, Lee HK, Jacobs RE, Lee S, Yi JH, Jo JM. Nuclear magnetic-resonance microscopy with 4-mu-m resolution – theoretical-study and experimental results. *Medical Physics* 1988;15(6):815.
- [26] Kuhn W. NMR Microscopy - Fundamentals, Limits and Possible Applications. *Angew. Chem. Int. Engl.* 1990;29(1):1–112.
- [27] Inglis BA, Yang L, Wirth ED, Plant D, Marceci TH. Diffusion Anisotropy in Excised Normal Rat Spinal Cord Measured by NMR Microscopy. *Magnetic Resonance Imaging* 1997;15(4):441–450.
- [28] Le Bihan D. Molecular diffusion, tissue microdynamics and microstructure. *NMR In Biomedicine* 1995;8(7-8):375.
- [29] Basser PL, Le Bihan D, Mattiello J. Measuring tissue fiber direction using diffusion NMR. *Biophysical Journal* 1993;64(2):A131.
- [30] Moonen CTW, Pekar J, de Vleeschouwer M H M, van Gelderen P, van Zijl P C M, DesPres D. Restricted and anisotropic displacement of water in healthy cat brain and in stroke studied by NMR diffusion imaging. *Magn. Reson. Med.* 1991;19:327–332.
- [31] Carr HY, Purcell EM. Effects of Diffusion on Free Precession in NMR Experiments. *Physical Review* 1954;94:630–638.
- [32] Stejskal EO, Tanner JE. Spin Diffusion Measurements in the Presence of Time-Dependent Field Gradient. *J. Chemical Physics* 1965;42:288.
- [33] Le Bihan D, Moonen CTW, Vanzijl PCM, Pekar J, Despres D. Measuring random microscopic motion of water in tissues with mr imaging – a cat brain study. *Journal of Computer Assisted Tomography* 1991;15(1):19.
- [34] Conturo TE, McKinstry RC, Akbudak E., Robinson, B.H., Encoding of Anisotropic Diffusion with Tetrahedral Gradients: A General Mathematical Diffusion Formalism and Experimental Results. *MRM* 1996;35:399–412.
- [35] Ahrens ET, Laidlaw D H, Readhead C, Brosnan C, Fraser S E, Jacobs R E. Magnetic resonance microscopy of transgenic mice that spontaneously acquire Experimental Allergic Encephalomyelitis. *MRM* 1998;40(1):119–132.
- [36] Kaufman MH, Lee KKH, Speirs S. Histological identification of primordial germ cells in diandric and digynic triploid mouse embryos. *Mol. Reprod. Devel.* 1990;25:364–368.
- [37] Moore SG. Pediatric Musculoskeletal Imaging. In: Stark DD, Bradley WG, editors. *Magnetic Resonance Imaging, 2*. St. Louis: Mosby-Year Book, 1992. pp. 2223.
- [38] Windham JP, Abd-Allah MA, Reimann DA, Froelich JW, Hagggar AM. Eigenimage Filtering in MR Imaging. *Journal of Computer Assisted Tomography* 1988;12(1):1–9.
- [39] Laidlaw, D.H., Barr, A.H., Jacobs, R.E., Goal-Directed Magnetic Resonance Brain Micro-Imaging. In: Koslow SH, Huerta MF, editors. *Neuroinformatics: An Overview of the Human Brain Projec.* Mahwah, NJ: Lawrence Erlbaum Assoc; 1996. p Chap. 5.
- [40] Watson, A.D., Rocklage, S.M., Carvlin, M.J., Contrast Agents. In: Stark DD, Bradley WG, editors. *Magnetic Resonance Imaging, Volume 1*. St. Louis: Mosby-Year Book, Inc.; 1992. p 372-437.
- [41] Runge VM, Carollo BR, Wolf CR, Nelson KL, Gelblum DY. Gd DTPA: a review of clinical indications in central nervous system magnetic resonance imaging. *Radiographics* 1989;9(5):929–958.
- [42] Jacobs, R. E., Fraser, S. E., *Imaging Neuronal Development with Magnetic Resonance Imaging (NMR) Microscopy*. In: Mize RR, Katz LC, editors. *Journal of Neuroscience Methods. Volume 54*. New York: Elsevier Press; 1994. p 189-196.
- [43] Moats RA, Fraser SE, Meade TJ A. “smart” magnetic resonance imaging agent that reports on specific enzymatic activity. *Angewandte Chemie-International Edition in English* 1997;36(7):726.
- [44] Bogdanov A, Weissleder R. The Development of in vivo imaging systems to study gene expression. *TIBTECH* 1998;16:5–10.
- [45] Wheeler DT, Schmidt R. The digital pathway: Multiphase development of a universal and expandable digital atlas of pathology. *Laboratory Investigation* 1997;76(1):1090.
- [46] Davidson D, Bard J, Brune R, Burger A, Dubreuil C, Hill W, Kaufman M, Quinn J, Stark M, Baldock R. The mouse atlas and graphical gene-expression database. *Seminars In Cell & Developmental Biology* 1997;8(5):509.
- [47] Roland PE, Zilles K. Brain Atlases – A New Research Tool. *TINS* 1994;17:458–467.

Russell Jacobs received his B.S. in Chemistry and Philosophy from Tulane University and his Ph.D. in Physical Chemistry from Stanford University. After a Post Doctoral Fellowship with Prof. Eric Oldfield at University of Illinois Urbana-Champaign spent building solid state NMR spectrometers and applying MR methods to the study of lipid-cholesterol and lipid-lipid interactions in bilayer membranes; he spent a year teaching and applying Raman spectroscopy methods to study membrane dynamics at Washington State University in Pullman, WA. He then moved to the Department of Physiology and Biophysics at the University of California Irvine where studies of the biophysics of lipid-peptide interactions were undertaken with a number of techniques. He is now a Member of the Beckman Institute at Caltech where his interests focus on elucidating mechanisms underlying important events in the development of the central nervous system and making magnetic resonance imaging microscopy a viable research tool.

Mary Dickinson is currently a post-doc at Caltech working on embryology and gene expression. She received her B.S. from Vanderbilt University in 1989 where she worked on mouse genetics and development and her Ph.D. from Columbia University in 1996. Her Ph.D. thesis included transgenic studies of cell proliferation in the spinal cord as well as a microsurgical analysis of neural crest induction in chick embryos. Dr. Dickinson has worked with a variety of organisms as an undergraduate, graduate student and as a teaching assistant at the Woods Hole Embryology course, but has settled on using chick and mouse embryos in her own research. Her major research interests include fluorescence imaging of cell movements and differentiation during development using two-photon and confocal laser scanning microscopy, developing 3-dimensional maps of gene expression and embryological development, and developing novel fluorescent dyes for use as probes in developing embryos.

Eric T. Ahrens received his B.S. in Physics from University of California at Los Angeles in 1988 and received his Ph.D. in Physics in 1994 from the same institution. His doctoral graduate research was conducted at the Condensed Matter and Thermal Physical Group at Los Alamos National Laboratory from 1990-1994 in the field of experimental condensed matter and low-temperature physics. In 1994, he became a Research Fellow in the Division of Biology at the California Institute of Technology, Pasadena, CA and is currently a Senior Research Fellow there. His research interests are in the area of applying in vivo magnetic resonance microscopy to a variety of biological problems and focuses on novel methods for visualizing the central nervous system.

David Laidlaw applies computer graphics and computer science to problems in other scientific disciplines. He is an Assistant Professor of Computer Science at Brown University. He received his Sc.B. and Sc.M. from Brown, where he worked with mathematicians to understand 2- and 3-manifolds. He received his Ph.D. in Computer Science from Caltech in 1995. His thesis presented new methods for extracting geometric models from medical imaging data of biological specimens. He is currently investigating computational methods with applications in developmental neurobiology, diagnostic medical imaging, remote sensing, and fluid mechanics. Research interests include tissue classification, visual representation of data, modeling of imaging data, optimization of data acquisition, geometry, numerical methods, and statistics.